nature energy

Article

https://doi.org/10.1038/s41560-025-01751-7

Rapid safety screening realized by accelerating rate calorimetry with lab-scale small batteries

Received: 2 September 2024

Accepted: 5 March 2025

Published online: 2 April 2025

Check for updates

Seongjae Ko[1,4], Hiromi Otsuka[2,4], Shin Kimura[2], Yuta Takagi[1], Shoji Yamaguchi[2], Takuya Masuda[2] ✉ & Atsuo Yamada[1,3] ✉

The increasing energy density and size requirements have necessitated the establishment of reliable safety technologies for rechargeable batteries. In particular, understanding and controlling thermal runaway, an uncontrollable heat generation from continuous exothermic reactions in batteries, is essential for developing high-safety batteries. However, comprehensive safety evaluations at the full-cell level are limited by size requirements (greater than the ampere-hour scale) for performing accelerating rate calorimetry tests that can provide critical information on heat generation during thermal runaway. Further, efficient safety screening is difficult because of substantial quantities of battery materials and costly manufacturing processes. Here we designed cylindrical pouch-type small batteries (~21 mAh, ~0.1 g of cathode active materials) that are highly susceptible to heat generation, thus allowing us to perform full-cell-level accelerating rate calorimetry tests on a laboratory scale. This enables rapid safety screening and early-stage feedback for battery design, which can help accelerate the development of high-safety batteries.

Rechargeable batteries (for example, Li-ion batteries) play a pivotal role in modern technology as they are used for powering consumer electronics and in industrial energy storage systems, both of which are essential for a sustainable green society[1–3]. Ensuring the safety and reliability of batteries has gained importance because of the increasing demand for higher energy density and larger size[4–7]. Thermal runway, which is a phenomenon where a rapid and uncontrollable temperature rise occurs because of continuous exothermic reactions in the battery, can cause catastrophic fires and explosions. Thus, understanding and controlling thermal runaway is essential to develop safe and reliable batteries[8,9]. However, progress in this direction has been extremely slow because of the complex nature of battery safety issues and the limitations of thermal runaway testing methods.

Over the past decades, extensive research has investigated several approaches to trace changes in the physico-chemical properties of individual battery components with increasing temperature caused by exothermic reactions at the material level using differential scanning calorimetry[10–15], X-ray diffraction[15–18] and gas chromatography-mass spectrometry[19–21]. These studies demonstrated that a sequential process, which includes the degradation of the solid–electrolyte interphase (SEI) on the anode surface[11,22]; direct reactions between the electrolyte and lithiated anode[12,13,18,23–25]; generation of Lewis acids, radicals and flammable gases via electrolyte decomposition[26–30]; and oxygen release with phase transitions in the cathode[31], can trigger and accelerate exothermic reactions to cause thermal runaway (Fig. 1).

Full-cell-level safety has been evaluated using various methods[32–34], including nail penetration, crush, drop, vibration, hotbox, thermal shock and accelerating rate calorimetry (ARC), to identify the risk for battery thermal runaway under external stress and/or drastic temperature changes. Among these methods, the ARC test offers quantitative

[1]The University of Tokyo, Bunkyo-ku, Japan. [2]Research Center for Energy and Environmental Materials (GREEN), National Institute for Materials Science (NIMS), Tsukuba, Japan. [3]Sungkyunkwan University Institute of Energy Science and Technology (SIEST), Sungkyunkwan University, Suwon-si, Korea. [4]These authors contributed equally: Seongjae Ko, Hiromi Otsuka. ✉e-mail: masuda.takuya@nims.go.jp; yamada@chemsys.t.u-tokyo.ac.jp

https://doi.org/10.1038/s41560-025-01751-7

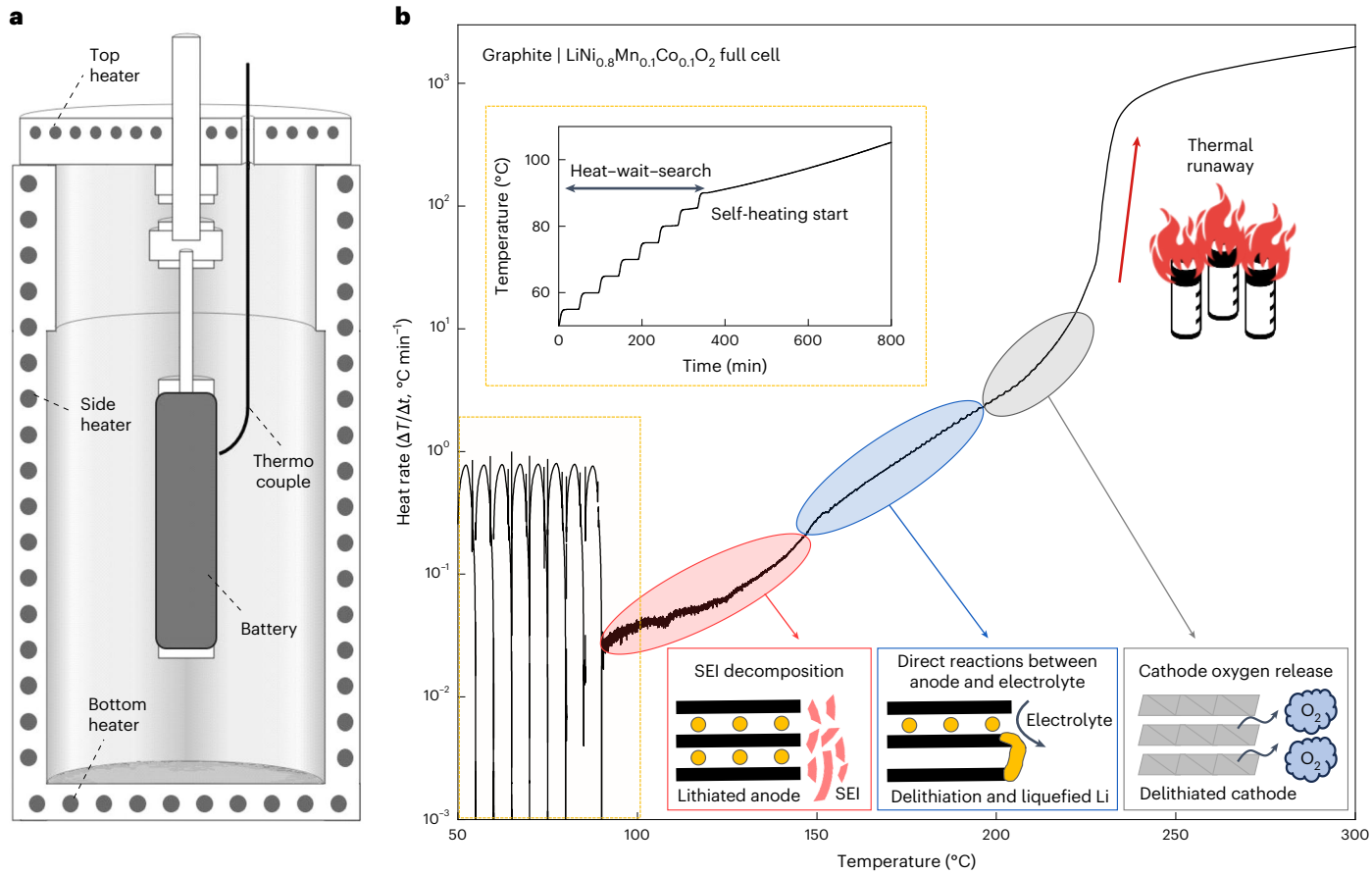

Fig. 1 | Detection of battery thermal runaway. a, Schematic of a typical ARC module used for full-cell-level safety evaluations. **b**, Representative ARC result, illustrating thermal runaway driven by continuous exothermic reactions in a graphite | $LiNi_{0.8}Mn_{0.1}Co_{0.1}O_2$ full cell. The insets present the heat rate–temperature (bottom-left yellow box) and temperature–time (top-left yellow box) graphs before and after battery self heating and sequential exothermic reactions occurring at the materials level; SEI decomposition (red box); direct reaction between lithiated anode, Li and electrolyte (blue box); and oxygen release from the cathode (grey box), which led to battery thermal runaway. The details of the ARC graph interpretation are presented in Supplementary Fig. 1. Credit: **a**, NETZSCH Japan.

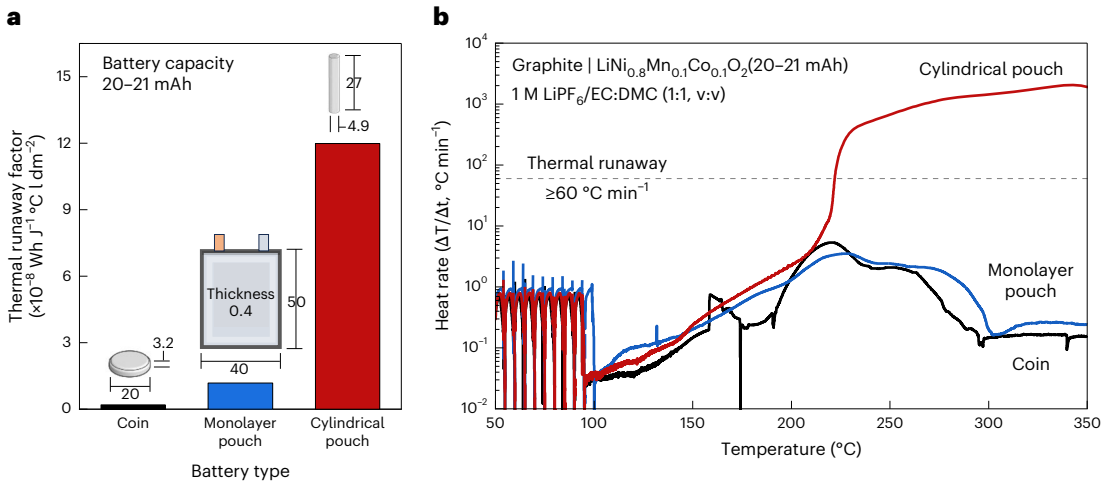

Fig. 2 | Successful observation of thermal runaway in a lab-scale small battery. a, Calculated TRFs of 0.2 (black), 1.2 (blue) and 12 (red) with almost identical capacities for cells composed of $LiNi_{0.8}Mn_{0.1}Co_{0.1}O_2$ cathode, graphite anode, ceramic-coated polyethylene separator and 1 M $LiPF_6$/ ethylene carbonate (EC):dimethyl carbonate (DMC) (1:1, v:v) electrolyte. The size of each battery is shown as insets in millimetres. **b**, ARC test results with three types of battery. The cells were charged to 4.2 V, discharged to 2.9 V as a formation process and then charged again to 4.2 V for the ARC test. The charge and discharge conditions were set to constant current–constant voltage (CC–CV, 0.1 C, 4.2 V, 1.5 h cut-off) for charging; constant current (CC, 0.1 C, 2.9 V cut-off) for discharging. The maximized TRF in the cylindrical pouch-type design enabled highly sensitive thermal runaway detection, even in a lab-scale 21 mAh small-capacity battery.

https://doi.org/10.1038/s41560-025-01751-7

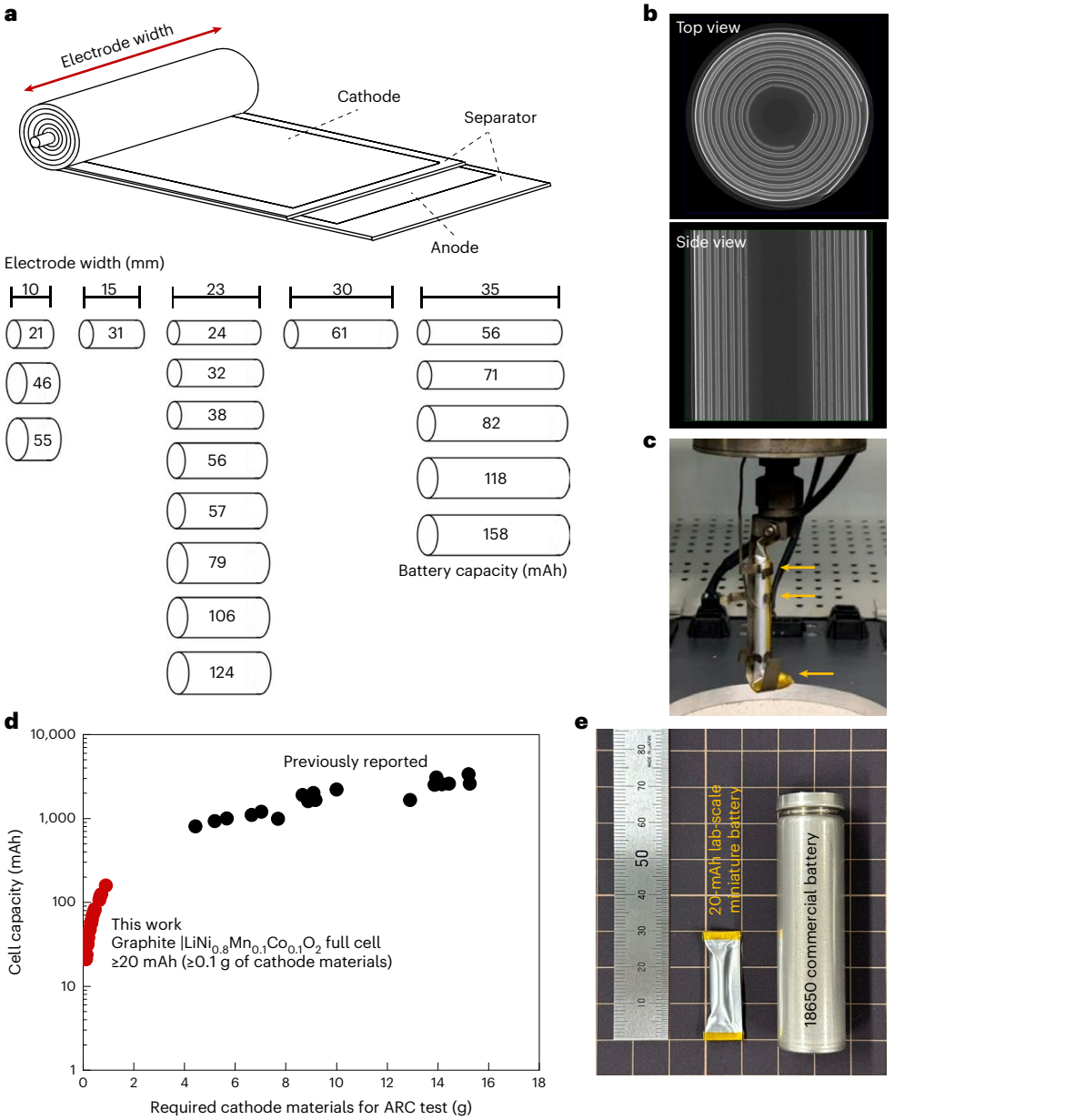

Fig. 3 | Design of cylindrical pouch-type cells. a–**c**, Schematic of the electrode and battery configuration with various cylindrical dimensions (**a**), images of a cylindrical pouch-type battery (31 mAh, 32 mm × 4.8 mm cylindrical cell with a 15 mm × 66 mm cathode) obtained via X-ray computed tomography (**b**) and ARC set-up (**c**); the prepared charged full cell (57 mAh, 40 mm × 7.5 mm cylindrical cell with a 23 mm × 80 mm cathode) was secured on a custom-made holder (stainless steel; SUS316, 0.1 mm thick) at three points (yellow arrows) to prevent detachment from the thermocouple during thermal runaway. **d**,**e**, Comparison of battery capacity and the amount of material resources (**d**) and sizes required for ARC tests (**e**). Credit: **c**, NETZSCH Japan.

values such as the onset temperature of battery self heating and thermal runaway and the related heat generation (Fig. 1 and Supplementary Fig. 1)[18,29,35–38]. In addition, variations in battery pressure and gases produced during thermal runaway can be monitored by incorporating pressure gauges and gas chromatography-mass spectrometry[18,39]. However, a full-cell-level ARC test requires ampere-hour (Ah)-scale batteries, necessitating expensive manufacturing processes that involve large quantities of materials[29,40–49]. These requirements hinder the efficient screening of battery materials and designs in the early stage of product development.

In this study, we design small cylindrical pouch-type cells (~21 mAh, ~0.1 g of cathode active materials) susceptible to heat generation to perform full-cell-level ARC tests on a laboratory scale. The ARC tests enable time- and cost-efficient safety screening for materials, cell design and operating conditions, expediting the development of high-safety batteries.

Theory of thermal runaway detection in an ARC test

Thermal runaway occurs when the generated heat exceeds the heat dissipation capacity of the battery, both of which are largely influenced by its design. Thus, the thermal runaway detection sensitivity can be maximized in the ARC test by considering battery design that minimizes heat dissipation (that is, intentionally design an unsafe battery), even when using lab-scale small batteries with a low capacity. Assuming that the battery is fabricated with the same electrodes and electrolyte (for example, cathode; $LiNi_{0.8}Mn_{0.1}Co_{0.1}O_2$/carbon/binder (94/3/3, w/w/w), anode; graphite/binder (93/7, w/w); ceramic-coated polyethylene separator; and 1 mol l^{-1} (M) $LiPF_6$/ethylene carbonate (EC):dimethyl carbonate (DMC) (1:1, v:v) electrolyte), the ratio of heat accumulation to dissipation is proportional to the ratio of battery energy (Wh) to the product of the specific heat (c_p, J g^{-1} °C^{-1}) and mass (m, g) of the battery

https://doi.org/10.1038/s41560-025-01751-7

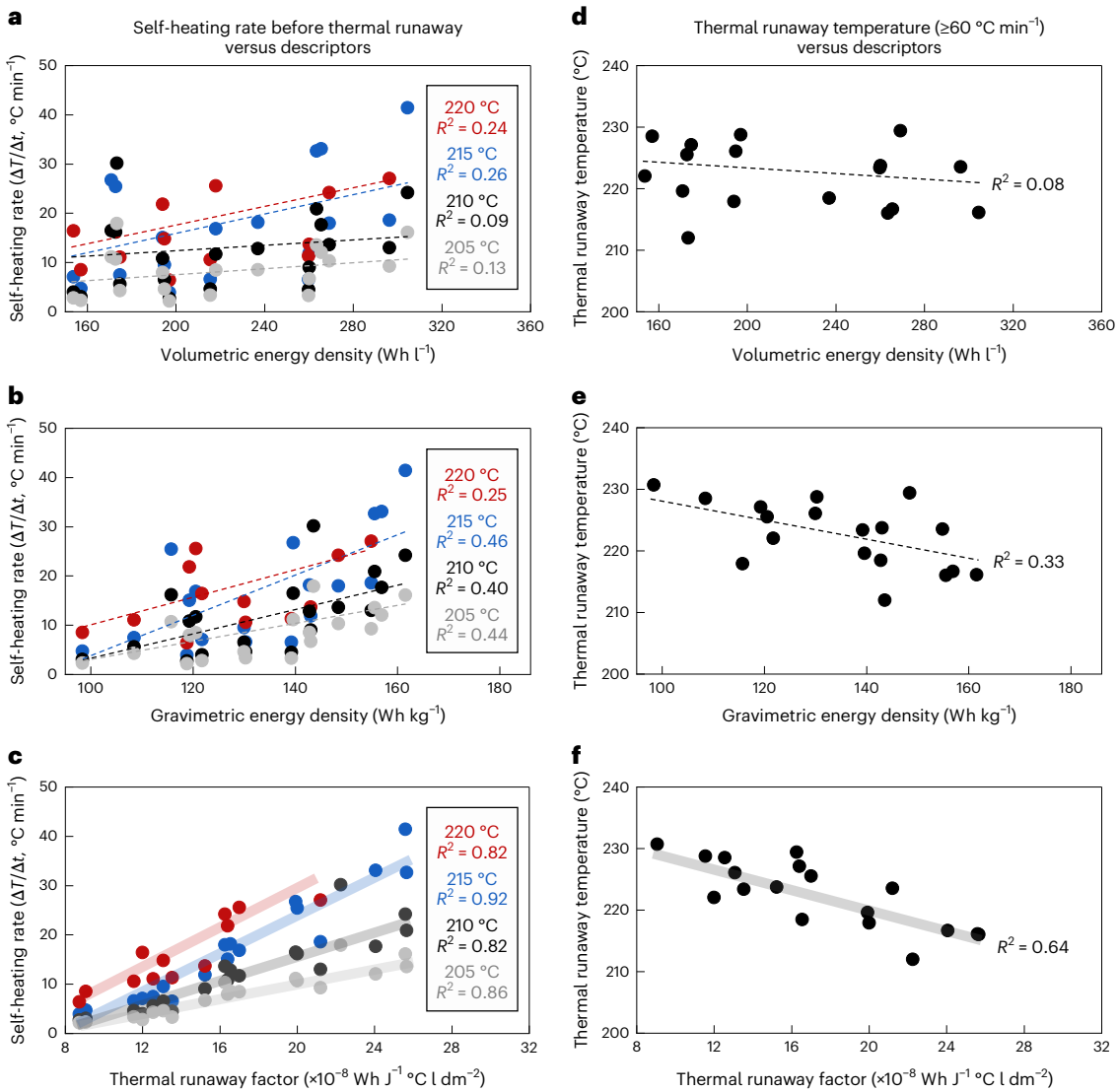

Fig. 4 | Battery safety as a function of TRF. a–**f**, Correlation of self-heating rates before thermal runaway (**a**–**c**) and onset temperature of thermal runaway with diverse descriptors (**d**–**f**). The TRF shows a better correlation with battery safety factors in ARC tests (**c** and **f**), compared with traditional descriptors such as volumetric and gravimetric energy densities (**a**, **b**, **d** and **e**). As guides to the eye, linear trend lines (dots or straight lines) using least squares regression are shown with the coefficient of determination (R^2).

components[25,49]. Then, the self-heating rate of the battery ($\Delta T/\Delta t$, °C min^{-1}) can be defined as

$$\Delta T/\Delta t \propto \frac{\mathrm{Wh}}{\sum(m \times c_\mathrm{p})} \quad (1)$$

Considering that the detection of the self-heating rate in the ARC test is affected by the heat transfer ability, which is diminished by the larger volume to surface area ratio (V/S, l dm^{-2}) of a heat-generating component (that is, battery electrode or jelly roll)[50], equation (1) can be modified as

$$\Delta T/\Delta t \propto \frac{\mathrm{Wh}}{\sum(m \times c_\mathrm{p})} \times \frac{V}{S} \quad (2)$$

Equation (2) represents the thermal runaway factor (TRF) crucial for detecting thermal runaway in lab-scale small batteries. The upper and lower terms of equation (2) are related to heat accumulation and dissipation into/from the battery, respectively.

Thermal runaway observation in a lab-scale small battery

The TRF values of the three lab-scale small batteries with similar capacities (20–21 mAh, prepared with 123–126 mg of cathode active material) are compared in Fig. 2a and Supplementary Table 1. The coin- and monolayer-pouch-type batteries demonstrate low TRFs because of the high heat capacities ($\sum(m \times c_\mathrm{p})$) of the battery package parts (cell case, wave spring, spacer and so on) and low V/S ratios (Supplementary Table 1). In contrast, the cylindrical pouch-type battery designed to maximize heat accumulation and minimize heat dissipation through a lower heat capacity and larger V/S ratio (Supplementary Table 1) exhibits a TRF that is more than ten times higher than those of the other batteries. These notable differences in TRF significantly affect the sensitivity of the ARC test. As shown in Fig. 2b, when the external temperature exceeds 90 °C, a self-heating process is initiated in all batteries by the thermal decomposition of the electrolyte and SEI on the anode[11,22]. However, thermal runaway starting at 220 °C induced by oxygen gas released from the charged $LiNi_{0.8}Mn_{0.1}Co_{0.1}O_2$ cathode active materials[31] was observed exclusively for the cylindrical pouch-type battery. Thus, TRF can be used as an effective descriptor to predict

https://doi.org/10.1038/s41560-025-01751-7

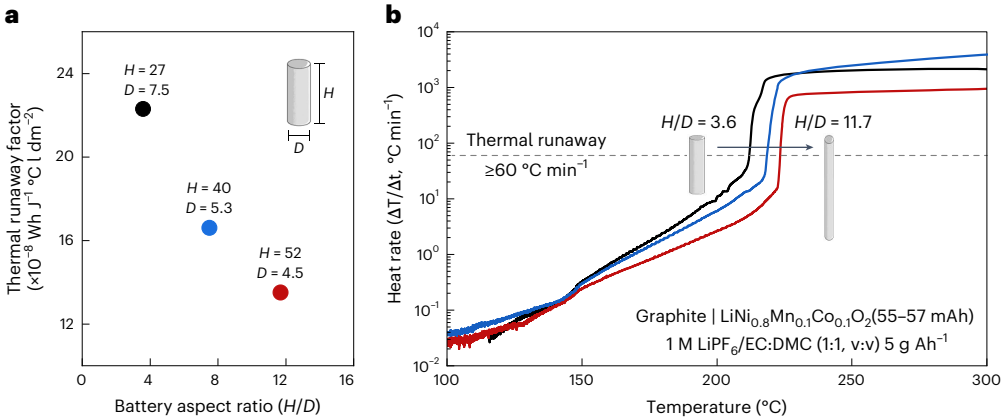

Fig. 5 | Effect of cell dimensions on battery safety. a,**b**, Calculated TRFs (**a**) and ARC results (**b**) for batteries with varying aspect ratios. The size of each battery is shown in millimetres. The cells were charged to 4.2 V, discharged to 2.9 V as a formation process and then charged again to 4.2 V for the ARC test. The charge and discharge conditions were set to constant current–constant voltage (CC–CV, 0.1 C, 4.2 V, 1.5 h cut-off) for charging; constant current (CC, 0.1 C, 2.9 V cut-off) for discharging. The onset temperature of thermal runaway is delayed by lowering the TRF through an increased *H*/*D* ratio of the battery.

battery safety, and its maximization can enable highly sensitive full-cell-level safety tests using minimal material resources. Note that in this study, a battery's self-heating rate exceeding 60 °C min^{-1} is selected as the criterion for thermal runaway, and the corresponding temperature is defined as the thermal runaway temperature (thermal runaway onset temperature). Although there is no strict definition or standard evaluation protocol for the thermal runaway of batteries, the set threshold (≥60 °C min^{-1}) encompasses all previously reported values for defining thermal runaway (Supplementary Fig. 1 and Supplementary Table 2).

Battery safety based on TRF

We fabricated 18 cylindrical pouch-type batteries with varying loading levels, electrodes and cell sizes to further investigate the relationship between TRF and battery safety (Fig. 3; note that all prepared cells have a TRF above 9, ensuring a sufficiently high self-heating rate to detect thermal runaway in the ARC test. The details of the electrode and cell design are provided in Supplementary Table 3). As illustrated in Fig. 4, the self-heating rate before thermal runaway and the onset temperature (under a common standard definition of ≥60 °C min^{-1}) showed a reasonable correlation with TRF and weak correlations with traditional descriptors such as volumetric and gravimetric energy densities. For example, the self-heating rate before thermal runaway has high coefficient of determination (R^2) values with TRF (0.82–0.92), and it largely outperforms those of conventional descriptors (0.09–0.26 for volumetric energy density and 0.25–0.46 for gravimetric energy density). The R^2 between the onset temperature of thermal runway and TRF was higher than that obtained with traditional descriptors, which highlights TRF as a simple yet reliable descriptor for battery safety, regardless of the definition of thermal runaway (Fig. 4 and Supplementary Figs. 2–4).

TRF not only helps observe thermal runaway in lab-scale small batteries with larger TRF for ARC tests but also offers valuable guidance in enhancing the safety of batteries by targeting smaller TRF. Equation (2) indicates that increasing the use of materials with high specific heat (c_p), such as electrolyte, current collector and separator (Supplementary Table 1), can lower TRF, potentially delaying thermal runaway. However, this approach sacrifices energy density and is impractical for achieving the ideal goal of simultaneously realizing both high energy density and high safety. We opted to design batteries with a high aspect ratio (height/diameter, *H*/*D*) to decrease the *V*/*S* ratio under nearly identical battery capacities of 55–57 mAh and electrolyte amounts of 5 g Ah^{-1}. As shown in Fig. 5 and Supplementary Fig. 5, changing the *H*/*D* ratio from 3.6 to 11.7 reduces the TRF from 22 to 14 and delays the onset temperature of thermal runaway from 212 to 223 °C. Therefore, designing batteries considering TRF is an effective approach to conduct full-cell-level ARC tests on lab-scale small batteries and provide critical insights to improve battery safety.

Safety screening of battery materials and cycling conditions

TRF supports effective safety screening for battery materials and operating conditions by increasing thermal runaway detection sensitivity in ARC tests. For instance, replacing the cathode active material high-Ni $LiNi_{0.8}Mn_{0.1}Co_{0.1}O_2$ (oxygen release from 220 °C) with the more thermally stable $LiNi_{0.5}Mn_{0.3}Co_{0.2}O_2$ containing less Ni (oxygen release from 250 °C) results in lower self-heating rates (Supplementary Fig. 6a)[31]. Conversely, introducing LiFSI ($LiN(SO_2F)_2$)-based salt-concentrated electrolytes, well known for their high oxidation and reduction stability, leads to higher self-heating rates due to exothermic chemical reactions between the LiFSI salt and the lithiated graphite anodes (Supplementary Fig. 6b)[12,13,18,23–25]. Furthermore, side reactions between the high-Ni $LiNi_{0.8}Mn_{0.1}Co_{0.1}O_2$ cathode and the electrolyte over long-term charge/discharge cycling give rise to increased internal resistance, electrolyte depletion and the generation of Lewis acids, radicals and flammable gases and cathode cracking, collectively heightening the thermal runaway risk (Supplementary Fig. 7)[29]. All of these findings indicate that battery self heating and thermal runaway from various factors can be detected sensitively and quantitatively in a time- and cost-efficient manner using TRF-engineered small cylindrical pouch-type cells in ARC tests. The facilitated full-cell-level ARC, combined with material-level differential scanning calorimetry and other safety-related protocols, will contribute to more efficient and comprehensive understanding of battery thermal runaway, thereby accelerating the development of high-energy-density, high-safety batteries.

Conclusions

In this study, a simple indicator for TRF was introduced to quantify the balance between heat accumulation and heat dissipation into/from batteries. Model experiments confirmed that designing batteries targeting a higher TRF can help in achieving precise control of the battery's heat balance, thereby lowering the detection thresholds for thermal runaway in ARC tests. Cylindrical pouch-type cells engineered for high TRF facilitate the observation of thermal runaway in full-cell-level ARC tests, even when using lab-scale miniature cells (~21 mAh, ~0.1 g of cathode active materials). This achievement is expected to accelerate the screening of battery safety across various materials, electrode/cell designs and operating conditions. Future research on validating the applicability of this approach to different battery chemistries is

expected to promote efficient product development with improved thermal management and reliability.

Methods

Electrode preparation

Cathode electrodes were prepared by coating a slurry of $LiNi_{0.8}Mn_{0.1}Co_{0.1}O_2$ or $LiNi_{0.5}Mn_{0.3}Co_{0.2}O_2$ (Hosen), acetylene black (HS100, Denka Black, Denka) and polyvinylidene fluoride (KF Polymer 1100, Kureha) in a weight ratio of 94:3:3 onto a 20-µm-thick aluminium (Al) foil (Fuji Impex). Subsequently, the coated foil was dried and densified using a roll press. Anode electrodes were purchased from Hosen and consisted of graphite and a polyvinylidene fluoride binder in a weight ratio of 93:7, coated on copper (Cu) foil. All electrodes were vacuum dried at 110 °C for 12 h before use.

Battery preparation

Coin-, monolayer-pouch- and cylindrical pouch-type batteries were fabricated considering several design parameters listed in Supplementary Tables 1 and 3. The coin-cell components (cathode can, anode can, gasket, wave washer and spacer) were purchased from Hosen. A ceramic-coated polyethylene separator (thickness: 16 ± 1.5 µm, Gurley value: 240 s 100 ml^{-1}) and a commercial electrolyte, 1 M $LiPF_6$/ethylene carbonate (EC):dimethyl carbonate (DMC) (solvent-to-solvent volume ratio 1:1, v:v) (Kishida) or LiFSI:DMC (salt-to-solvent molar ratio 1:1.9, *n*:*n*) were used. The jelly rolls for cylindrical pouch batteries were prepared by winding the electrodes and separator, as illustrated in Fig. 3. X-ray computed tomography was conducted to visualize the internal structure of the cylindrical pouch-type battery using a Zeiss Xradia 520 with a tube voltage of 150 kV, 10 W and an exposure time of 3.0 s.

Specific heat measurement

All samples (active materials; delithiated $LiNi_{0.8}Mn_{0.1}Co_{0.1}O_2$, delithiated $LiNi_{0.5}Mn_{0.3}Co_{0.2}O_2$ and lithiated graphite powders, separator, electrolytes, current collectors; Al and Cu foils and packages; coin-cell components and Al pouches) were sealed in aluminium pans in an Ar-filled glovebox. The active materials (delithiated $LiNi_{0.8}Mn_{0.1}Co_{0.1}O_2$, delithiated $LiNi_{0.5}Mn_{0.3}Co_{0.2}O_2$ and lithiated graphite) were collected by disassembling Li|$LiNi_{0.8}Mn_{0.1}Co_{0.1}O_2$, Li|$LiNi_{0.5}Mn_{0.3}Co_{0.2}O_2$ and Li|graphite cells. The measurement was performed using a differential scanning calorimeter (3500 Sirius, NETZSCH) with sapphire (φ 5.2 mm, *t* 0.75 mm, 62.62 mg) as the standard reference material, from −20 to +35 °C at a heating rate of 10 °C min^{-1} under N_2 flow (100 ml min^{-1}).

ARC test

Full cells with various designs were charged and discharged once to check the battery capacity and then charged again for the ARC test using a battery charge–discharge machine (HJ1001SD8, Hokuto Denko Corporation). The charge and discharge conditions are controlled as follows: constant current (0.1 C, 4.2 V cut-off)/constant voltage (4.2 V, 1.5 h) for charging and constant current (0.1 C, 2.9 V cut-off) for discharging. The C-rate was calculated based on the measured capacity of the active materials (176 mAh g^{-1}). The measurement was performed using a NETZSCH MMC274 in an Ar-filled glovebox to ensure that the thermal runaway results are attributable only to the battery and not influenced by external air contamination. The detailed ARC test conditions are presented in Supplementary Fig. 1.

Data availability

Data related to the experimental procedures, materials and battery design information are available in the article and its Supporting Information. Source data are provided with this paper.

References

1. Yoshino, A. The birth of the lithium-ion battery. *Angew. Chem. Int. Ed.* **51**, 5798–5800 (2012).
2. Kim, T., Song, W., Son, D.-Y., Ono, L. K. & Qi, Y. Lithium-ion batteries: outlook on present, future, and hybridized technologies. *J. Mater. Chem. A* **7**, 2942–2964 (2019).
3. Armand, M. & Tarascon, J.-M. Building better batteries. *Nature* **451**, 652–657 (2008).
4. Bandhauer, T. M., Garimella, S. & Fuller, T. F. A critical review of thermal issues in lithium-ion batteries. *J. Electrochem. Soc.* **158**, R1–R25 (2011).
5. Lisbona, D. & Snee, T. A review of hazards associated with primary lithium and lithium-ion batteries. *Process Saf. Environ. Prot.* **89**, 434–442 (2011).
6. Doughty, D. & Roth, E. P. A general discussion of Li Ion battery safety. *Electrochem. Soc. Interface* **21**, 37–44 (2012).
7. Chen, Y. et al. A review of lithium-ion battery safety concerns: the issues, strategies, and testing standards. *J. Energy Chem.* **59**, 83–99 (2021).
8. Wang, Q. et al. Thermal runaway caused fire and explosion of lithium ion battery. *J. Power Sources* **208**, 210–224 (2012).
9. Wang, Y. et al. Challenges and opportunities to mitigate the catastrophic thermal runaway of high-energy batteries. *Adv. Energy Mater.* **13**, 2203841 (2023).
10. Spotnitz, R. & Franklin, J. Abuse behavior of high-power, lithium-ion cells. *J. Power Sources* **113**, 81–100 (2003).
11. Lee, H. H., Wan, C. C. & Wang, Y. Y. Thermal stability of the solid electrolyte interface on carbon electrodes of lithium batteries. *J. Electrochem. Soc.* **151**, A542 (2004).
12. Yamaki, J. Thermal stability of graphite anode with electrolyte in lithium-ion cells. *Solid State Ionics* **148**, 241–245 (2002).
13. Joho, F., Novák, P. & Spahr, M. E. Safety aspects of graphite negative electrode materials for lithium-ion batteries. *J. Electrochem. Soc.* **149**, A1020 (2002).
14. Edström, K. et al. Carbon electrode morphology and thermal stability of the passivation layer. *J. Power Sources* **97–98**, 87–91 (2001).
15. Yamaki, J. et al. Thermal stability of electrolytes with Li_xCoO_2 cathode or lithiated carbon anode. *J. Power Sources* **119–121**, 789–793 (2003).
16. Hu, E. et al. Oxygen-release-related thermal stability and decomposition pathways of $Li_xNi_{0.5}Mn_{1.5}O_4$ cathode materials. *Chem. Mater.* **26**, 1108–1118 (2014).
17. Andersson, A. S., Thomas, J. O., Kalska, B. & Häggström, L. Thermal stability of $LiFePO_4$-based cathodes. *Electrochem. Solid-State Lett.* **3**, 66–68 (2000).
18. Liu, X. et al. In situ observation of thermal-driven degradation and safety concerns of lithiated graphite anode. *Nat. Commun.* **12**, 4235 (2021).
19. Kahr, J., Groher, C., Schierer, V., Rosenberg, E. & Jahn, M. Operando gas chromatography mass spectrometry for the continuous study of overcharge-induced electrolyte decomposition in lithium-ion batteries. *J. Power Sources* **615**, 235038 (2024).
20. Gachot, G. et al. Gas chromatography/Fourier transform infrared/mass spectrometry coupling: a tool for Li-ion battery safety field investigation. *Anal. Methods* **6**, 6120–6124 (2014).
21. Gachot, G. et al. Gas chromatography/mass spectrometry as a suitable tool for the li-ion battery electrolyte degradation mechanisms study. *Anal. Chem.* **83**, 478–485 (2011).
22. Ryou, M.-H. et al. Effects of lithium salts on thermal stabilities of lithium alkyl carbonates in SEI layer. *Electrochim. Acta* **83**, 259–263 (2012).
23. Wang, Q., Sun, J., Yao, X. & Chen, C. Thermal behavior of lithiated graphite with electrolyte in lithium-ion batteries. *J. Electrochem. Soc.* **153**, 329–333 (2006).

24. Andersson, A. M., Herstedt, M., Bishop, A. G. & Edström, K. The influence of lithium salt on the interfacial reactions controlling the thermal stability of graphite anodes. *Electrochim. Acta* **47**, 1885–1898 (2002).
25. Yang, H., Bang, H., Amine, K. & Prakash, J. Investigations of the exothermic reactions of natural graphite anode for li-ion batteries during thermal runaway. *J. Electrochem. Soc.* **152**, A73 (2005).
26. Xu, K. Nonaqueous liquid electrolytes for lithium-based rechargeable batteries. *Chem. Rev.* **104**, 4303–4418 (2004).
27. Arbizzani, C., Gabrielli, G. & Mastragostino, M. Thermal stability and flammability of electrolytes for lithium-ion batteries. *J. Power Sources* **196**, 4801–4805 (2011).
28. Campion, C. L., Li, W. & Lucht, B. L. Thermal decomposition of $LiPF_6$-based electrolytes for lithium-ion batteries. *J. Electrochem. Soc.* **152**, A2327 (2005).
29. Hou, J. et al. Thermal runaway of Lithium-ion batteries employing $LiN(SO_2F)_2$-based concentrated electrolytes. *Nat. Commun.* **11**, 5100 (2020).
30. Ravdel, B. et al. Thermal stability of lithium-ion battery electrolytes. *J. Power Sources* **119–121**, 805–810 (2003).
31. Sharifi-Asl, S., Lu, J., Amine, K. & Shahbazian-Yassar, R. Oxygen release degradation in li-ion battery cathode materials: mechanisms and mitigating approaches. *Adv. Energy Mater.* **9**, 1900551 (2019).
32. Jaguemont, J. & Bardé, F. A critical review of lithium-ion battery safety testing and standards. *Appl. Therm. Eng.* **231**, 121014 (2023).
33. Lin, C. et al. Deep-dive analysis of the latest lithium-ion battery safety testing standards and regulations in Germany and China. *Renew. Sustain. Energy Rev.* **173**, 113077 (2023).
34. Feng, X. et al. Thermal runaway mechanism of lithium ion battery for electric vehicles: a review. *Energy Storage Mater.* **10**, 246–267 (2018).
35. Liu, X. et al. Thermal runaway of lithium-ion batteries without internal short circuit. *Joule* **2**, 2047–2064 (2018).
36. Richard, M. N. & Dahn, J. R. Accelerating rate calorimetry studies of the effect of binder type on the thermal stability of a lithiated mesocarbon microbead material in electrolyte. *J. Power Sources* **83**, 71–74 (1999).
37. Richard, M. N. & Dahn, J. R. Accelerating rate calorimetry study on the thermal stability of lithium intercalated graphite in electrolyte. II. modeling the results and predicting differential scanning calorimeter curves. *J. Electrochem. Soc.* **146**, 2078–2084 (1999).
38. MacNeil, D. D., Larcher, D. & Dahn, J. R. Comparison of the reactivity of various carbon electrode materials with electrolyte at elevated temperature. *J. Electrochem. Soc.* **146**, 3596–3602 (1999).
39. Li, Y. et al. Pressure effect on the thermal runaway behaviors of lithium-ion battery in confined space. *Fire Technol.* **59**, 1137–1155 (2023).
40. He, T. et al. An investigation on thermal runaway behaviour of a cylindrical lithium-ion battery under different states of charge based on thermal tests and a three-dimensional thermal runaway model. *J. Cleaner Prod.* **388**, 135980 (2023).
41. Mendoza-Hernandez, O. S., Ishikawa, H., Nishikawa, Y., Maruyama, Y. & Umeda, M. Cathode material comparison of thermal runaway behavior of Li-ion cells at different state of charges including over charge. *J. Power Sources* **280**, 499–504 (2015).
42. Duh, Y.-S. et al. Characterization on thermal runaway of commercial 18650 lithium-ion batteries used in electric vehicles: a review. *J. Energy Storage* **41**, 102888 (2021).
43. Lei, B. et al. Experimental analysis of thermal runaway in 18650 cylindrical Li-ion cells using an accelerating rate calorimeter. *Batteries* **3**, 14 (2017).
44. Barkholtz, H. M. et al. Multi-scale thermal stability study of commercial lithium-ion batteries as a function of cathode chemistry and state-of-charge. *J. Power Sources* **435**, 226777 (2019).
45. Ishikawa, H., Mendoza, O., Sone, Y. & Umeda, M. Study of thermal deterioration of lithium-ion secondary cell using an accelerated rate calorimeter (ARC) and AC impedance method. *J. Power Sources* **198**, 236–242 (2012).
46. Hou, J. et al. Thermal runaway of lithium-ion batteries employing flame-retardant fluorinated electrolytes. *Energy Environ. Mater* **6**, e12297 (2023).
47. Duh, Y.-S., Tsai, M.-T. & Kao, C.-S. Thermal runaway on 18650 lithium-ion batteries containing cathode materials with and without the coating of self-terminated oligomers with hyper-branched architecture (STOBA) used in electric vehicles. *J. Therm. Anal. Calorim.* **129**, 1935–1948 (2017).
48. Jhu, C.-Y., Wang, Y.-W., Wen, C.-Y. & Shu, C.-M. Thermal runaway potential of $LiCoO_2$ and $Li(Ni_{1/3}Co_{1/3}Mn_{1/3})O_2$ batteries determined with adiabatic calorimetry methodology. *Appl. Energy* **100**, 127–131 (2012).
49. Son, K. et al. Comparative study of thermal runaway and cell failure of lab-scale Li-ion batteries using accelerating rate calorimetry. *J. Ind. Eng. Chem.* **83**, 247–251 (2020).
50. Planinšič, G. & Vollmer, M. The surface-to-volume ratio in thermal physics: from cheese cube physics to animal metabolism. *Eur. J. Phys.* **29**, 369–384 (2008).

Acknowledgements

This work was supported by the Japan Science and Technology Agency Program on Open Innovation Platform for Industry-Academia Co-Creation (grant number JPMJPF2016) and the Japan Society for the Promotion of Science Grant-in-Aid for Scientific Research (grant number 20H05673).

Author contributions

A.Y. conceived and initiated the research. A.Y. and T.M. co-managed the project. S. Ko and H.O. designed the TRF parameter. H.O., S. Ko, S. Kimura and Y.T. conducted the experiments. S.Y. contributed to the ARC set-up. S. Ko drafted the paper, and A.Y. contributed to its editing.

Competing interests

The authors declare no competing interests.

Additional information

Supplementary information The online version contains supplementary material available at https://doi.org/10.1038/s41560-025-01751-7.

Correspondence and requests for materials should be addressed to Takuya Masuda or Atsuo Yamada.

Peer review information *Nature Energy* thanks Palani Balaya and Mark Buckwell for their contribution to the peer review of this work.